

Supporting Information for

3D Imaging of Transition Metals in the Zebrafish Embryo by X-ray Fluorescence Microtomography

Daisy Bourassa,^a Sophie-Charlotte Gleber,^b Stefan Vogt,^b Hong Yi,^c Fabian Will,^d Heiko
Richter,^d Chong Hyun Shin,^e Christoph J. Fahrni^{a*}

^a*School of Chemistry and Biochemistry and Petit Institute for Bioengineering and Bioscience, Georgia Institute of Technology, 901 Atlantic Drive, Atlanta, GA 30332, USA.* ^b*Advanced Photon Source, X-ray Science Division, Argonne National Laboratory, 9700 S. Cass Avenue, Argonne, IL 60439, USA.* ^c*Robert P. Apkarian Integrated Electron Microscopy Core, Emory University, 1521 Dickey Drive, Atlanta, GA 30322, USA.* ^d*LLS Rowiak LaserLabSolutions GmbH, Garbsener Landstrasse 10, D-30419 Hannover, Germany.* ^e*School of Biology and Petit Institute for Bioengineering and Bioscience, Georgia Institute of Technology, 310 Ferst Drive, Atlanta, GA 30332, USA*

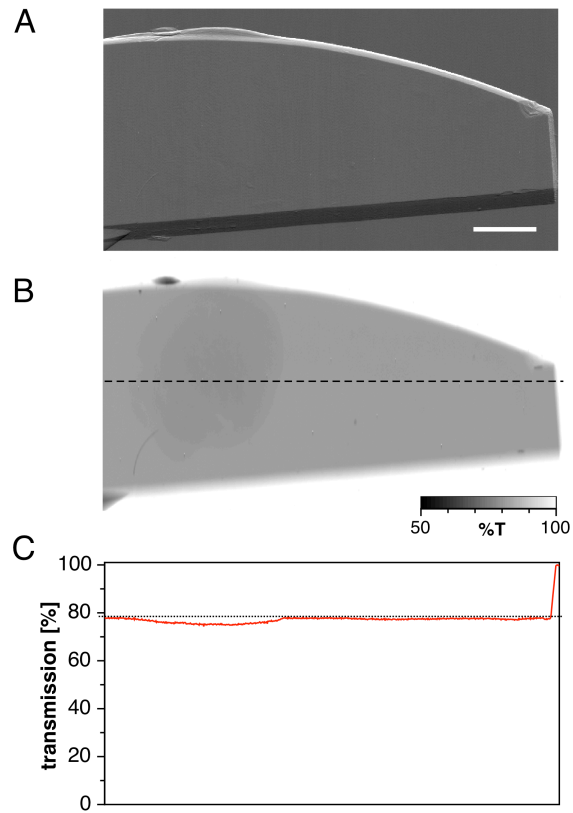


Figure S1: Evaluation of the incident beam attenuation by the sample. A) Horizontal phase contrast image¹ of the resin block with embedded zebrafish embryo. Scale bar: 200 μm . B) Absorption contrast image for a projection angle of 90 deg. The gray scale represents the transmitted fraction of the excitation intensity based on the ratio of the photon count recorded at the upstream vs. downstream ion chambers. C) Transmission profile for the trace indicated as dashed line in B). The dotted line corresponds to the transmission level of the Lowicryl resin.

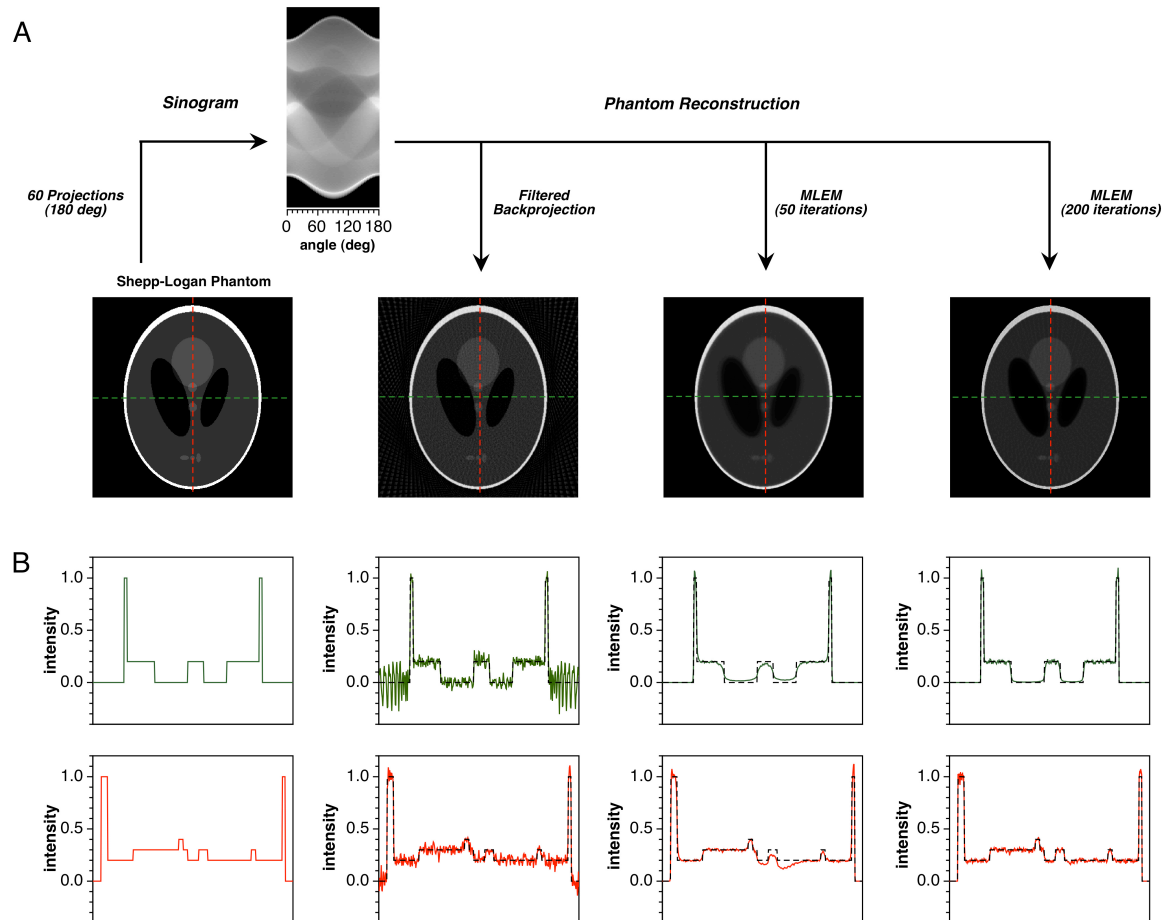


Figure S2: Reconstruction of a Shepp-Logan phantom based on filtered backprojection (“Ram-Lak” ramp filter) or iterative maximum likelihood expectation maximization (MLEM) algorithms. A) A sinogram was constructed from the phantom (1st column) based on 60 projections spaced over 180 degrees. The original image was reconstructed either through the filtered backprojection (2nd column) or MLEM with 50 and 200 iterations (3rd and 4th column), respectively. B) Comparison of the intensity profiles of the original phantom and the reconstructed images. The position of the profiles is indicated in each image by the color-coded green and red traces.

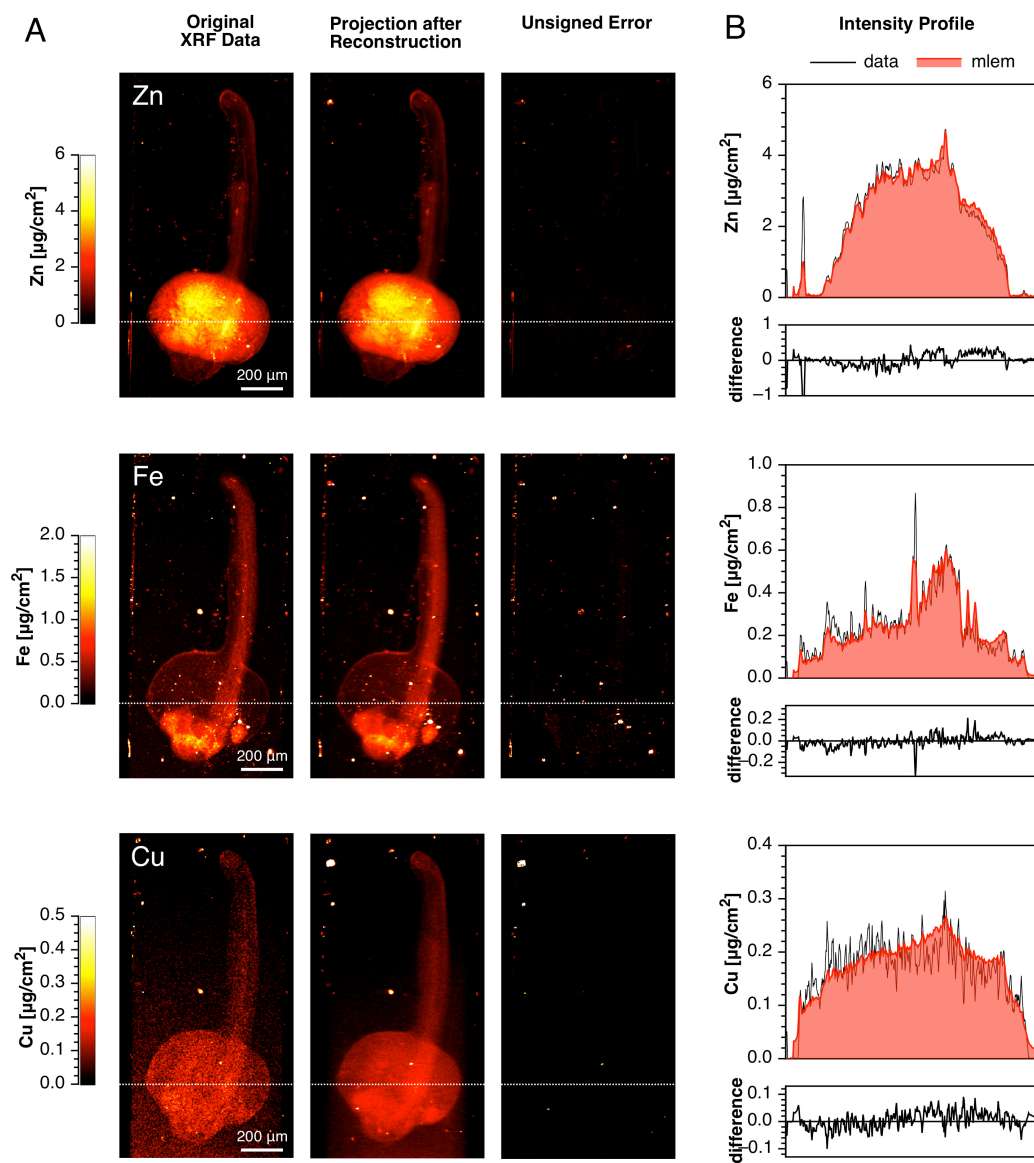


Figure S3: Comparison of the experimental and reconstructed data for the first projection at 0 degree. A) The volumetric distribution of each element was reconstructed using the iterative maximum likelihood expectation maximization (MLEM) algorithm, and the reconstructed data were projected at the same angle as the measured data (2nd column). The 3rd column illustrates the unsigned error in the form of difference images. The panels for each element are based on different density scales as indicated by the calibration bars on the left. B) Intensity profiles of the experimental (black) and reconstructed data (red) across the dashed line indicated in the projection images. The graph below each profile illustrates the signed difference between the experimental and reconstructed profiles.

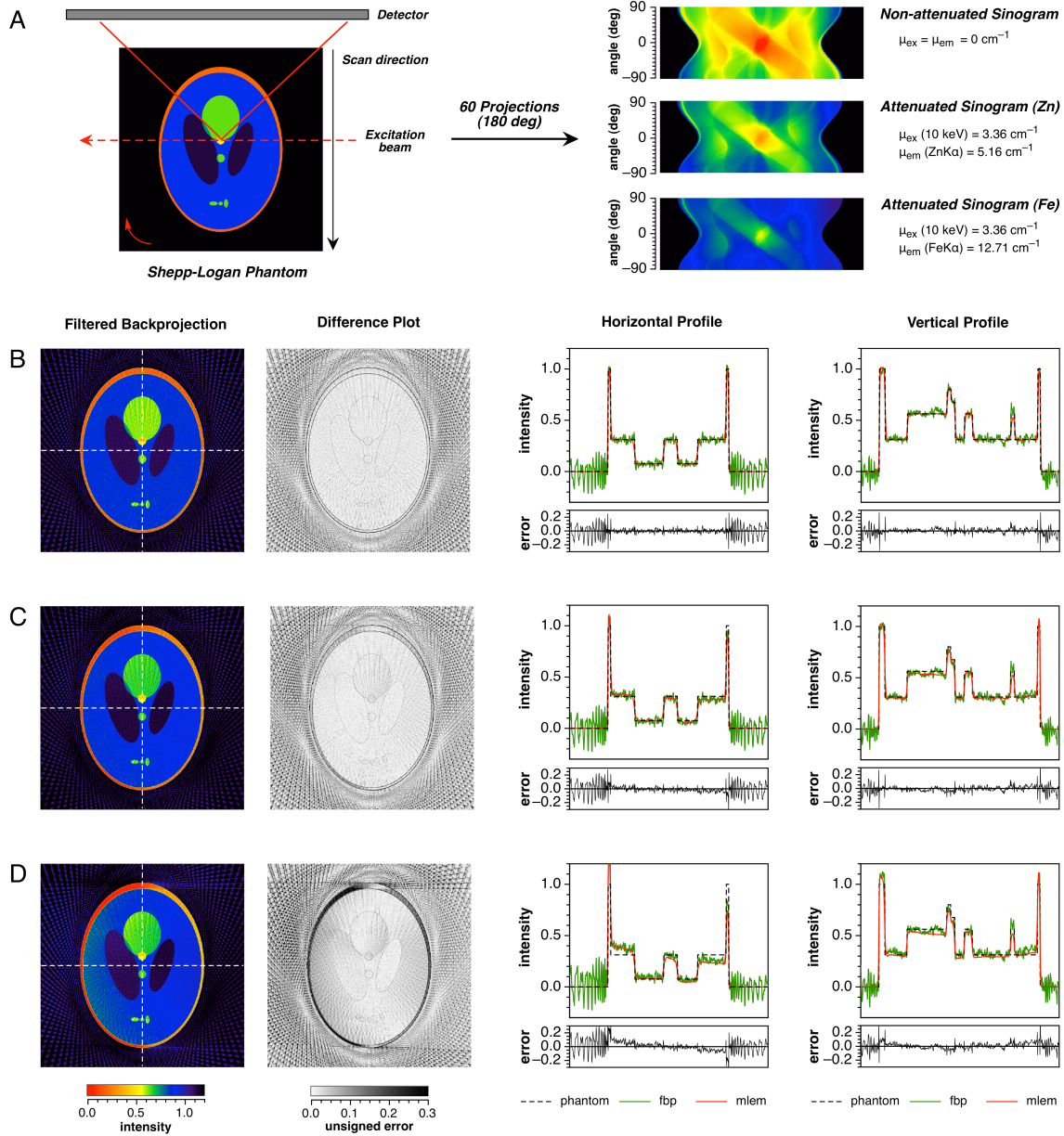


Figure S4: Error evaluation for attenuation correction by linear scaling. A) Phantom image and geometry of the fluorescence tomography setup. A set of two attenuated and a non-attenuated sinogram was computed using the *raft* C-library software.² Specifically, an attenuation matrix of $680 \times 680 \mu\text{m}$ was applied with uniform attenuation coefficients for excitation ($\mu_{\text{ex}}(10 \text{ keV}) = 3.96 \text{ cm}^{-1}$) and emission ($\mu_{\text{ZnK}\alpha} = 6.09 \text{ cm}^{-1}$ or $\mu_{\text{FeK}\alpha} = 15.00 \text{ cm}^{-1}$). Filtered back projections and errors were computed for the non-attenuated sinogram (B), and for the attenuated sinograms with Zn K α emission (C) and Fe K α emission (D), respectively. The reconstructed images (B) and (C) were adjusted by the corresponding scaling factors f calculated based on equation S2. The difference plots (absolute values) were obtained by subtracting the reconstructed images from the original phantom. The position of the intensity profiles on the right is indicated in each image as white traces. In addition to the filtered back projection data (green traces), the intensity profiles show the MLEM data (red traces) obtained from reconstruction of the attenuated sinograms and the original phantom profile (dashed black traces).

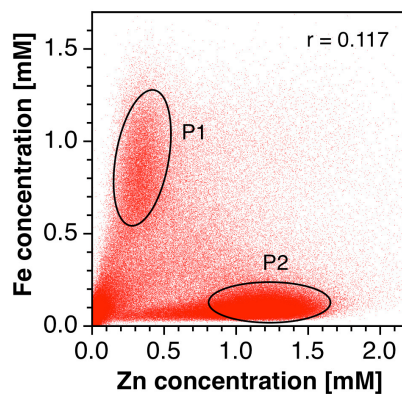


Figure S5: Scatter plot illustrating the correlation between the Zn and Fe distribution in a zebrafish embryo at 24 hpf. Each pixel indicates the elemental concentration of a voxel in the reconstructed data set. Due to the large size of the original data set, the voxels were binned by a factor of 64 to yield a total of 1.95 million pixels. The Pearson's correlation coefficient r was calculated based on the binned data set.

Attenuation Correction Based on Linear Scaling Factors

The attenuation of X-rays with incident intensity I_0 by a material of thickness x is described by the Beer-Lambert law (S1),

$$I(x) = I_0 e^{-\mu x} \quad (\text{S1})$$

where μ is the energy-dependent linear attenuation coefficient of the material. If the attenuation is dominated by the embedding material, the attenuation of exciting and emitting photons at the center of rotation remains approximately constant throughout all projections, and the corresponding scaling factor f can be expressed as

$$f = e^{(\mu_{ex} + \mu_{em})l/2} \quad (\text{S2})$$

where l is the mean attenuation pathlength, and μ_{ex} and μ_{em} are the linear attenuation coefficients of the material at the corresponding excitation and emission energies, respectively. Because the attenuation coefficients of Lowicryl for excitation and emission in the 5-10 keV range are relatively small, we reasoned that a simple linear attenuation correction might still provide reasonable estimates of the elemental concentrations in the reconstructed volumetric model, albeit with some deviations across the xz-plane as illustrated with Fig. S4.

The actual elemental concentration c_0 can be expressed by equation (S3)

$$c_0 = c_{us} \cdot e^{(\mu_{ex} + \mu_{em})l/2} \quad (\text{S3})$$

where c_{us} denotes the reconstructed elemental concentrations derived from projections that were calibrated based on the upstream ion chamber photon flux. Because the downstream ion chamber calibration can compensate for some of the attenuation differences within a projection, we estimated the actual concentrations c_0 based on the downstream-calibrated concentrations c_{ds} . For this purpose, we combined equation (S3) with relationship (S4)

$$c_{us} = c_{ds} \cdot e^{-l\mu_{ex}} \quad (\text{S4})$$

and derived scaling factors f for each element according to equation (S5)

$$c_0 = f \cdot c_{ds} \quad \text{with} \quad f = e^{(\mu_{em} - \mu_{ex})l/2} \quad (\text{S5})$$

The corresponding attenuation coefficients of Lowicryl were determined based on the NIST values for polymethyl methacrylate (PMMA, density 1.18 g/cm³) using the software WinXCOM,³⁻⁵ and the pathlength l was derived based on equation (1) of the main text using the corresponding integrated Zn densities averaged over all projections. With μ_{ex} (10 keV) = 3.96 cm⁻¹, $\mu_{\text{ZnK}\alpha}$ = 6.09 cm⁻¹, $\mu_{\text{CuK}\alpha}$ = 7.52 cm⁻¹, $\mu_{\text{FeK}\alpha}$ = 15.00 cm⁻¹, and a mean pathlength of l = 680 μm , we obtained the scaling factors f of 1.08, 1.13, and 1.46 for Zn, Cu, and Fe, respectively.

References

- (1) Hornberger, B.; De Jonge, M. D.; Feser, M.; Holl, P.; Holzner, C.; Jacobsen, C.; Legnini, D.; Paterson, D.; Rehak, P.; Struder, L., "Differential phase contrast with a segmented detector in a scanning X-ray microprobe", *J. Synchrotron Rad.* **2008**, *15*, 355-362.
- (2) Miqueles, E. X.; De Pierro, A. R., "C-library raft: Reconstruction algorithms for tomography. Applications to X-ray fluorescence tomography", *Comp. Phys. Commun.* **2011**, *182*, 2661-2673.
- (3) Gerward, L.; Guilbert, N.; Jensen, K. B.; Levring, H., "WinXCom: A program for calculating X-ray attenuation coefficients", *Radiation Phys. Chem.* **2004**, *71*, 653-654.
- (4) Gerward, L.; Guilbert, N.; Bjørn Jensen, K.; Levring, H., "X-ray absorption in matter. Reengineering XCOM", *Radiation Phys. Chem.* **2001**, *60*, 23-24.
- (5) Berger, M. J.; Hubbell, J. H., "XCOM: photon cross sections database, Web Version 1.2 (1999), available at <http://physics.nist.gov/xcom>. National Institute of Standards and Technology, Gaithersburg, MD 20899, USA. (Originally published as NBSIR 87-3597 (1987): "XCOM: Photon Cross Sections on a Personal Computer")".